

Appendix C:
**Effect of Relative Humidity on the Detection of Sulfur Dioxide
and Sulfuric Acid Using a Chemical Ionization Mass
Spectrometer***

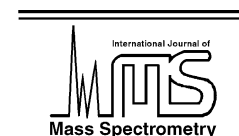
* This chapter is reproduced by permission from "Effect of Relative Humidity on the Detection of Sulfur Dioxide and Sulfuric Acid Using a Chemical Ionization Mass Spectrometer" D. Salcedo, P. W. Villalta, V. Varutbangkul, J. C. Wormhoudt, R. C. Miake-Lye, D. R. Worsnop, J. O. Ballenthin, W. F. Thorn, A. A. Viggiano, T. M. Miller, R. C. Flagan, J. H. Seinfeld, *International Journal of Mass Spectrometry*, 231 (1): 17-30, 2004. Copyright 2004, Elsevier, Ltd.



ELSEVIER

SCIENCE @ DIRECT®

International Journal of Mass Spectrometry 231 (2004) 17–30



www.elsevier.com/locate/ijms

Effect of relative humidity on the detection of sulfur dioxide and sulfuric acid using a chemical ionization mass spectrometer

D. Salcedo^{a,1}, P.W. Villalta^{b,2}, V. Varutbangkul^a, J.C. Wormhoudt^b,
R.C. Miake-Lye^b, D.R. Worsnop^b, J.O. Ballenthin^c, W.F. Thorn^c,
A.A. Viggiano^c, T.M. Miller^c, R.C. Flagan^a, J.H. Seinfeld^{a,*}

^a Chemical Engineering Department, California Institute of Technology, Pasadena, CA 91125, USA

^b Aerodyne Research Inc., Billerica, MA, USA

^c Air Force Research Laboratory, Hanscom Air Force, Hanscom, MA, USA

Received 9 June 2003; accepted 5 September 2003

Abstract

Detection of sulfur dioxide and sulfuric acid at high relative humidity was studied using a chemical ionization mass spectrometer (CIMS). The reactant ions used in the experiments are $\text{CO}_3^- \cdot n\text{H}_2\text{O}$ ($n = 0-5$), which react with SO_2 to form $\text{SO}_5^- \cdot n\text{H}_2\text{O}$ ($n = 0-2$). H_2SO_4 reacts with the precursor ions to form HSO_4^- ($m/z = 97$ amu) and $\text{H}_2\text{SO}_4 \cdot \text{CO}_3^-$ ($m/z = 158$ amu). We report the first use of the latter ionization scheme to detect sulfuric acid. High RH affects the detection of SO_2 and H_2SO_4 by forming clusters with the reactant and product ions, reducing sensitivity. Increasing the temperature breaks these clusters. For SO_2 at high RH, either SO_5^- ($m/z = 112$ amu) or $\text{SO}_5^- \cdot \text{H}_2\text{O}$ ($m/z = 130$ amu) can be used for SO_2 detection without a decrease in sensitivity. For H_2SO_4 at high RH, it is preferred to detect the ion $\text{H}_2\text{SO}_4 \cdot \text{CO}_3^-$ because the background signal at 158 amu is small, and a better sensitivity can be achieved.

© 2003 Elsevier B.V. All rights reserved.

Keywords: Chemical ionization mass spectrometer; Sulfur dioxide; Sulfuric acid; Water clusters; Relative humidity

1. Introduction

The predominant anthropogenic sulfur-containing compound directly emitted into the atmosphere is sulfur dioxide, the atmospheric oxidation of which produces sulfuric acid [1]. Sulfuric acid has been implicated in the formation of new particles in the atmosphere through nucleation in combination with water and possibly ammonia [2], and it can also promote the growth of pre-existing particles by condensation on their surfaces. Once these particles reach a few hundred nanometers in diameter they might have a significant impact on the formation of clouds and regulation of global climate through efficient scattering of sunlight [3].

SO_2 is emitted predominantly through fossil fuel combustion and is also a major oxidation product of reduced sulfur compounds in the atmosphere, such as dimethyl sulfide (DMS) [1]. Mixing ratios of sulfur dioxide in continental background air range from 20 ppt to over 1 ppb. In the unpolluted marine boundary layer levels range between 20 and 50 ppt. Urban SO_2 mixing ratios can attain values of several hundred parts per billion [4].

Sulfuric acid vapor in the atmosphere is mainly a product of the gas-phase oxidation of SO_2 by the hydroxyl (OH) radical [5,6]:



Field measurements show a strong diurnal variation in H_2SO_4 tracking the UV solar flux, which drives the formation of OH. Since H_2SO_4 has a very low vapor pressure (below 10^{-12} atm [7]), once formed, it tends to condense

* Corresponding author. Tel.: +1-626-3954-635; fax: +1-626-7962-591.

E-mail address: seinfeld@caltech.edu (J.H. Seinfeld).

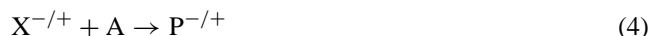
¹ Present address: Departamento de Ingeniería y Ciencias Químicas, Universidad Iberoamericana, México, DF, Mexico.

² Present address: University of Minnesota Cancer Center, Minneapolis, MN, USA.

rapidly into the aerosol phase; consequently, its concentration in the gas phase is very low: rural continental and marine air levels range from a few ppq (parts per quadrillion, or parts in 10^{15}) at night to 1.2 ppt at mid-day [8,9].

Atmospheric SO_2 can be measured using several techniques. These include: gas chromatography with flame photometric detection (FPD) (detection limit (DL) = 0.1–0.3 ppb); ultraviolet fluorescence (DL < 0.3 ppt); [10] differential optical absorption spectrometry (DOAS) (DL = 10–100 ppt), tunable diode laser spectroscopy (TDLS) (DL = 0.5 ppb), and Fourier-transform infrared spectrometry (FTIR) (DL = 25 ppb, falling to 0.01 ppb with sample concentration using Matrix Isolation) [11]. Chemical ionization mass spectrometry (CIMS) has also been used to measure SO_2 in the troposphere (DL = 1 ppb [12] and 0.5 ppt [13–16]). The only in-situ atmospheric measurements of sulfuric acid have been carried out using CIMS. Arnold and Fabian in 1980 published the first measurement of sulfuric acid in the stratosphere [17]. The first measurement of H_2SO_4 in the troposphere was reported by Eisele and Tanner in 1993 [18].

In chemical ionization, the analyte molecules (A) are ionized via ion/molecule reactions:



Both the precursor ($\text{X}^{-/+}$) and the product ($\text{P}^{-/+}$) ions are analyzed with a mass spectrometer. If the concentration of the precursor ion is much higher than that of the product ion, and if the reaction time and rate of reaction are known, the concentration of A can be calculated from the ratio of the signals of $\text{X}^{-/+}$ and $\text{P}^{-/+}$. The selectivity of this technique is determined by the selection of a suitable precursor ion, which reacts with the species of interest, but does not react with the major atmospheric species. The soft ionization technique, which results in little molecular fragmentation, and the selectivity of the ion/molecule reactions significantly reduce interferences and simplify interpretation of the mass spectra, compared with other commonly used techniques such as electron impact ionization. Furthermore, CIMS is very sensitive because the ion/molecule reactions are generally fast, often approaching collision-controlled kinetics [19].

When CIMS instruments are used at high relative humidity (such as in the troposphere), water molecules tend to form clusters with the ions present in the gas phase (with product ions, as well as with precursor ions), which is undesirable for several reasons. The reaction rates of the clusters depend on the number of water molecules attached. Some reaction rates increase when one or two molecules of water are attached to the bare ion [20,21]. However, rate constants typically decrease with increasing hydration number [22,23]. Furthermore, if the product ions form hydrates, the total signal partitions into many smaller signals due to the hydrates, decreasing the instrument sensitivity. Finally, some of the clustered ions present might have the same mass as one of the product ions, increasing the background signal.

A compact CIMS instrument has been developed at the Air Force Research Laboratory (AFRL at the Hanscom Air Force Base in Massachusetts). The instrument has been used to measure a variety of atmospheric species, including ambient SO_2 [12,24,25]. Here, we used a new version of the spectrometer designed and developed by AFRL, and built by Aerodyne Research, Inc. (ARI). We describe its performance to detect SO_2 and H_2SO_4 in high-humidity environments and discuss the interferences caused by water-clustering. A new ionization scheme for sulfuric acid is proposed, based on the product ion $\text{H}_2\text{SO}_4 \cdot \text{CO}_3^-$.

2. Chemical ionization mass spectrometer

The CIMS used in this work is a variant of the instrument developed by the group at AFRL. In this section, we present only a brief description of the instrument, because it is similar to that previously described in the literature [12,24,26]. Fig. 1 shows a diagram of the instrument. Most parts were custom made, except for components such as pressure and temperature gauges and vacuum pumps.

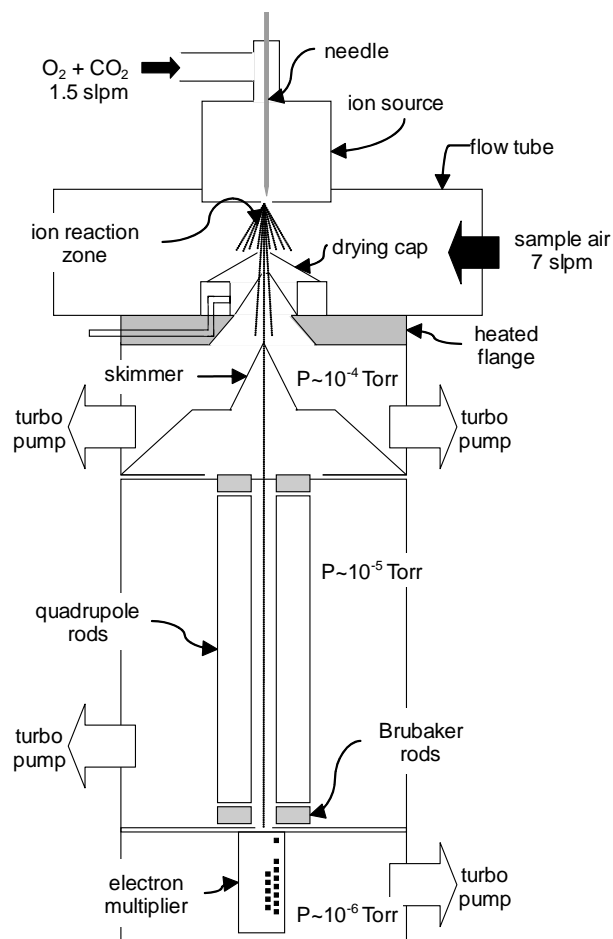


Fig. 1. Schematic of the CIMS instrument.

2.1. Mass spectrometer

The ion mass analyzer consists of three chambers made of aluminum to reduce weight, which are differentially pumped with turbo pumps (Varian 300HT, Lexington, MA, USA). The first region is open to the flow-tube through an orifice of 100 μm in diameter, to which a negative potential is applied to steer the ions into the chamber. The bulk of the gas passing through the orifice is pumped away with two turbo pumps, which are backed up by a diaphragm pump (Vacuubrand MD4, Wertheim, Germany) to keep the pressure of the first chamber at about 10^{-4} Torr. A conical nickel skimmer with a 1.5-mm orifice separates the first chamber from the second one, which is at a pressure of about 10^{-5} Torr. This region contains a quadrupole mass filter to separate the ions as a function of their mass to charge ratio. The stainless steel quadrupole rods, which were custom made at the AFRL, are 9.53 mm in diameter and 18.73 cm long. An additional set of rods (4.1 cm-long at the entrance of the quadrupole and 1.27 cm at the exit), to which only the radio-frequency voltage is applied (Brubaker lenses), are present to reduce the adverse effects of fringing fields in the instrument sensitivity [27]. The mass spectrometer has a mass range of 1–210 amu with a 1 amu resolution. Finally, the third region contains a discrete-dynode electron multiplier (ETP Electron Multipliers Pty Ltd., Sydney, Australia) for ion counting. The pressure in the last chamber is about 10^{-6} Torr. The two back chambers are pumped with two turbo pumps that are backed by the two pumps connected to the first chamber.

Compact custom electronics produced by AFRL power and control the quadrupole rods and electron multiplier. An external laptop computer running the instrument control software is used as an interface to an on-board microprocessor that controls all the functions of the mass spectrometer (ion lens tuning, mass resolution, multiplier gain, discriminator level, etc.). Such functions, as well as the sequence of measurements, can all be preprogrammed. The code for the instrument control was written at the AFRL in FortH Language. The compiled program runs on OS/2 operation system.

2.2. Ion source

The ion source is located directly opposite to the inlet to the mass spectrometer. It consists of a steel needle inserted into an aluminum cup, remaining about 5 mm from an orifice 1.2 mm in diameter. A potential of about -2.5 to -3.0 kV is applied to the needle while 1.5 slpm of oxygen (Air Liquide, 99.993% pure) is passed through the cup with a small amount of CO_2 (<1%), to generate a corona discharge between the tip of the needle and the exit of the orifice. The pressure in the discharge is typically 290 Torr. Free electrons from the discharge attach to oxygen to form O_2^- and O^- ions, which react quickly with O_2 , O_3 , and CO_2 to generate CO_3^- , the precursor ion (see Section 3).

2.3. Flow-tube

The flow-tube consists of a square channel made of aluminum connecting the ion source and the mass spectrometer. Sampled air flows transversely to the ion source at a rate of 7 slpm. The reaction region is that in which the sampled air and the oxygen from the ion source intersect and the ion products are formed. The ions reach the entrance of the mass spectrometer carried by the oxygen jet coming out from the ion source and by the electric field generated by the voltages applied to the mass spectrometer entrance. A pressure of approximately 200 Torr is maintained in the flow-tube.

As will be discussed later, high relative humidity reduces the sensitivity of the instrument by forming water clusters with the reactant and product ions. Initially, in order to reduce ion–water clustering, the sampling orifice of the mass spectrometer was preceded by a drying cap with a 3 mm hole into which heated gas could be injected to break the water clusters. The heating of the gas was accomplished by cartridge heaters embedded in the copper flange holding the mass spectrometer sampling orifice. With this configuration, the temperature of the entire flow-tube increased because the heated flange is not thermally insulated. In this work, the temperature reported is that measured at the copper flange. The largest temperature gradient along the flow-tube is $\sim 10^\circ\text{C}$. A small negative potential applied to the drying cap helps to guide the ions through the cap. Most of the experiments with SO_2 were performed using this configuration. However, it was determined that the increase in temperature of the flow-tube was sufficient to break the water clusters, and no drying gas was used in the described experiments. For the experiments at 150°C , the drying cap was removed (see next paragraph), but it was determined that the sensitivity of the CIMS to SO_2 at lower temperatures was not affected by this change.

Sulfuric acid is a “sticky” molecule that is easily lost to surfaces, and extreme care is necessary to keep sulfuric acid from adsorbing to the walls. Initially, the instrument exhibited a slow decay (few hours) of the sulfuric acid signal after the flow of sulfuric acid into the flow-tube was stopped, due to desorption from surfaces. The desorbing time was reduced to 10 min by increasing the temperature of the flow-tube to 150°C and by removing the drying cap. The drying cap was mounted on a ceramic ring which prevented uniform heating and whose porosity may have made it an effective sink for sulfuric acid.

2.4. Water, SO_2 , and H_2SO_4 sources

Fig. 2 shows a diagram of the flow system used to introduce gases into the CIMS flow-tube. Unless otherwise noted, UHP nitrogen (Air Liquide, Paris, France) was used as carrier gas. Water concentration in the flow-tube was controlled by saturating a portion of the N_2 flow with a water-bubbler and changing the relative flows of dry and humid N_2 . Mixing ratios of water in the flow-tube were converted into relative

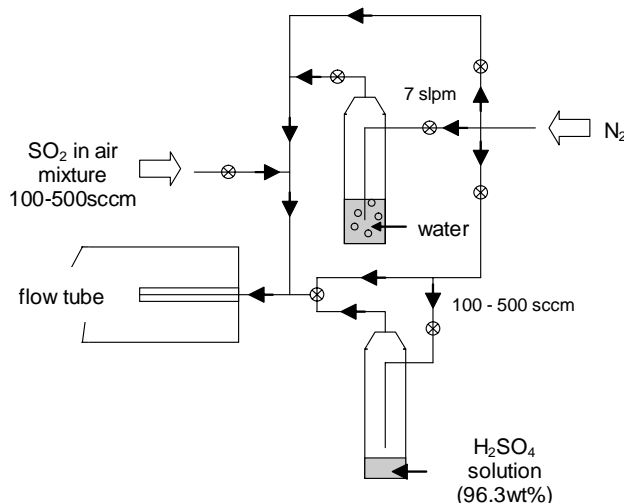


Fig. 2. Schematic of the flow system and water, SO₂, and sulfuric acid sources.

humidity at 20 °C and 1 atm (which are the values reported throughout this paper) in order to correlate the results to sampled ambient air.

A certified mixture of SO₂ and air (0.997 ppm SO₂ in balance air; Scott Specialty Gases, Plumsteadville, PA, USA) was used as the source of SO₂.

Commercial calibrated sources of gaseous sulfuric acid are not available; hence, a source of sulfuric acid had to be designed. It consists of an impinger, the bottom of which is filled with a 96.3 wt.% solution of sulfuric acid (ACS Reagent, J.T. Baker, Phillipsburg, NJ, USA). A measured flow of nitrogen gas was passed over the surface of the liquid while monitoring the solution temperature. The saturation degree of the H₂SO₄ vapor in the N₂ flow was calculated using a model of the impinging gas flow field developed by Allen et al. [28]. Using vapor pressures of sulfuric from the model by Carslaw et al. [7], the concentration of sulfuric acid in the flow-tube was computed. With this information and the flow rates used, the concentration of sulfuric acid can be computed. The inlet to introduce the sulfuric acid in the flow-tube consists of a 0.25 in. o.d. and 0.15 in. i.d. quartz tube wrapped with a heating wire. Another glass tube (0.5 in. o.d.) was used around the inner tube in order to connect the inlet to the flow-tube with an Ultra-Torr fitting (Swagelok, Solon, OH, USA). All the lines and valves connecting the impinger to the flow-tube are either Teflon or glass treated with a hydrophobic coating (T2494 from United Chemical Technologies, Bristol, PA, USA) to reduce the absorption of sulfuric acid to the walls. Heating tapes are used to keep all the lines at 120–150 °C.

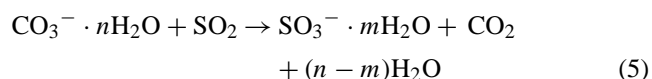
The source of sulfuric acid described above has two main uncertainties: losses of sulfuric acid to the walls of the inlet and the flow-tube; and the accuracy of the impinger model for H₂SO₄ entrainment. Without another quantitative way of measuring sulfuric acid, we are unable to determine the value of these uncertainties. However, for the purpose of this

paper (to describe the interferences caused by high relative humidity) we only require a source that delivers a reproducible amount of sulfuric acid. In Section 4.3 we show that the signal due to sulfuric acid is reproducible.

3. Chemical ionization

Negative ions in the discharge are formed by termolecular electron attachment to O₂, forming O₂⁻·O⁻ is also formed by dissociative attachment. O₂⁻ and O⁻ undergo a series of ion/molecule reactions with O₂ and O₃ (formed in the discharge) that convert them into O₃⁻ [29]. If CO₂ is added to the discharge, O₃⁻ reacts rapidly with it, and CO₃⁻ becomes the main ion produced. Other ions that are formed in the discharge to a minor extent (<0.1%) include OH⁻, O₄⁻, and CO₄⁻. In the presence of water vapor, all of these ions associate with H₂O molecules in the gas phase to form equilibrium distributions of hydrates (X⁻·nH₂O). Table 1 lists the reaction rate constants of relevant reactions of O₃⁻·nH₂O and CO₃⁻·nH₂O with SO₂ and H₂SO₄.

SO₂ is ionized by the following O⁻ transfer reaction:

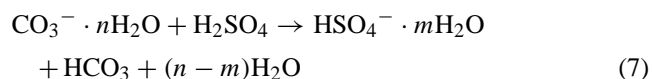


O₃⁻ can also react with SO₂ in a similar manner to form SO₃⁻. The products of the reactions of O₂⁻·nH₂O with SO₂ are SO₂⁻ and SO₄⁻. In the presence of oxygen, reaction (5) is followed by the rapid conversion of the SO₃⁻ ions into SO₅⁻:



Reaction (5) has been studied by Albritton et al. [30] for $n = 0$. Möhler et al. [31] studied reaction (5) for $n = 0, 1$ at 298 K. Seeley et al. [32] measured the reactions rates between 158 and 600 K for $n = 0$, and for $1 \leq n \leq 5$ at 300 K and below. These three reports agree under the conditions where their measurements overlap. The rate constant for reaction (5) depends on the number of water molecules attached to the CO₃⁻ ion. The rate constant increases by approximately a factor of 2 with the addition of a single water molecule, but decreases for $n > 3$ [32]. As a result, the ionization efficiency of SO₂ depends on the humidity conditions, which determines the reactant-ion/hydrates equilibrium.

Viggiano et al. [21] measured the rate constants for the reactions of sulfuric acid with several ions commonly used in CIMS. Of importance here is the following reaction:



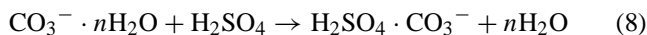
for $0 < n < 2$. The rate constant of reaction (7) at 300 K was found to be independent of the hydration number for CO₃⁻.

Table 1
Rates of reaction of relevant ions with SO₂, H₂SO₄, and SO₃

Reaction	Rate constant at 300 K (cm ³ molecule ⁻¹ s ⁻¹)	Reference
SO ₂ + O ₃ ⁻ → SO ₃ ⁻ + O ₂	1.90 × 10 ⁻⁹	[31]
SO ₂ + O ₃ ⁻ · H ₂ O → Products	1.80 × 10 ⁻⁹	[31]
SO ₂ + O ₃ ⁻ · 2H ₂ O → Products	1.70 × 10 ⁻⁹	[31]
SO ₂ + CO ₃ ⁻ → SO ₃ ⁻ + CO ₂	0.37 × 10 ⁻⁹ ^a 0.48 × 10 ⁻⁹	[32] [31]
SO ₂ + CO ₃ ⁻ · H ₂ O → SO ₃ ⁻ · nH ₂ O + CO ₂ + (1 - n)H ₂ O	1.60 × 10 ⁻⁹ 1.40 × 10 ⁻⁹	[32] [31]
SO ₂ + CO ₃ ⁻ · 2H ₂ O → SO ₃ ⁻ · nH ₂ O + CO ₂ + (2 - n)H ₂ O	1.60 × 10 ⁻⁹	[32]
SO ₂ + CO ₃ ⁻ · 3H ₂ O → SO ₃ ⁻ · nH ₂ O + CO ₂ + (3 - n)H ₂ O	1.40 × 10 ⁻⁹	[32]
SO ₂ + CO ₃ ⁻ · 4H ₂ O → SO ₃ ⁻ · nH ₂ O + CO ₂ + (4 - n)H ₂ O	0.38 × 10 ⁻⁹	[32]
SO ₂ + CO ₃ ⁻ · 5H ₂ O → SO ₃ ⁻ · nH ₂ O + CO ₂ + (5 - n)H ₂ O	0.28 × 10 ⁻⁹	[32]
H ₂ SO ₄ + CO ₃ ⁻ → HSO ₄ ⁻ + HCO ₃	2.39 × 10 ⁻⁹	[21]
H ₂ SO ₄ + CO ₃ ⁻ · H ₂ O → HSO ₄ ⁻ + HCO ₃ + (1 - n)H ₂ O	2.15 × 10 ⁻⁹	[21]
H ₂ SO ₄ + CO ₃ ⁻ · 2H ₂ O → HSO ₄ ⁻ + HCO ₃ + (2 - n)H ₂ O	2.39 × 10 ⁻⁹	[21]
SO ₃ + CO ₃ ⁻ → SO ₄ ⁻ + CO ₂	1.00 × 10 ⁻⁹	[36]

^a Temperature dependence $k = 0.37(300/T)^{1.27}$.

The following reaction occurring between CO₃⁻ and H₂SO₄ was reported by Villalta et al. [33]:



with a branching ratio between reactions (7) and (8) of 0.7 and 0.3, respectively, at a temperature of the ionization region of 90 °C and a pressure of 60–130 Torr. To our knowledge, the rate of reaction (8) has not been previously measured, and this is the first report of using reaction (8) as the ionization scheme for sulfuric acid.

The sensitivity of the instrument is the signal obtained normalized to the concentration of the analyte, and it depends on the reaction time, pressure in the flow-tube, and ion/molecule reaction rate. For good performance, it is necessary to find the conditions that maximize the sensitivity. It is also very important to reduce the background signal at the m/z of interest as much as possible to improve the DL of the instrument. The DL is the minimum concentration of the analyte necessary to obtain a signal exceeding the noise of the background signal and the electronic noise, and it is calculated using the sensitivity of the instrument, the background signal, and the integration time. If a longer integration time is used, the statistical noise decreases and a better DL can be achieved. The DL must be reported along with the sensitivity to describe the performance of the instrument, because a large sensitivity might not be enough for detection if the noise is also large.

4. Results and discussion

4.1. Effect of RH in background spectra

Fig. 3 shows background spectra obtained under four different conditions. Spectrum A was taken while no CO₂ was added to the ion source. In this case the dominant ion formed

in the discharge is O₃⁻·H₂O. Some CO₃⁻ is also formed due to impurities. When CO₂ is introduced in the ion source (spectrum B), the predominant ion formed is CO₃⁻. Clusters of CO₃⁻ with water and nitrogen are also present in smaller quantities. Spectra C and D illustrate the effect of adding water vapor to the flow-tube and heating the flow-tube. Spectrum C was obtained at 7% RH and room temperature. Under these conditions, CO₃⁻ is still predominantly formed; however, it is clustered by water molecules. Increasing the temperature of the flow-tube breaks the clusters, especially those with more than two water molecules (spectrum D).

The effect of water on the spectra is shown in more detail in Figs. 4 and 5, which show data taken at room temperature (~20 °C). In Fig. 4 the ion signal of each CO₃⁻ hydrate (CO₃⁻·nH₂O) is shown as a function of number of water molecules in the hydrate (n) at different RH values. The distribution of the hydrates shifts towards higher n as RH increases. Fig. 5 shows the signal of each hydrate, as well as the sum of all the hydrates ($n = 0-6$), as a function of RH. The total CO₃⁻ ion signal ($\sum \text{CO}_3^- \cdot n\text{H}_2\text{O}$, $n = 0-6$) remains practically constant at the lower RH because the formation of water clusters occurs in the flow-tube after the CO₃⁻ ions have been formed, and only the equilibrium among the clusters is affected. As RH increases, the total signal of CO₃⁻ decreases because the transmission of the ions through the quadrupole decreases with ion mass. Therefore, the larger CO₃⁻ hydrates, which dominate the ion population, are not transmitted as efficiently as the smaller hydrates. The total ion signal for CO₃⁻ does not decrease appreciably until RH > 10. Before that, the main CO₃⁻ hydrates present have $n = 0-4$. Therefore, ions with mass up to 132 amu (corresponding to CO₃⁻·4H₂O) must be efficiently transmitted through the quadrupole.

When compared to Fig. 3C, Fig. 3D shows that the hydration of ions in the flow-tube can be reduced by increasing the temperature of the flow-tube. Although the concentra-

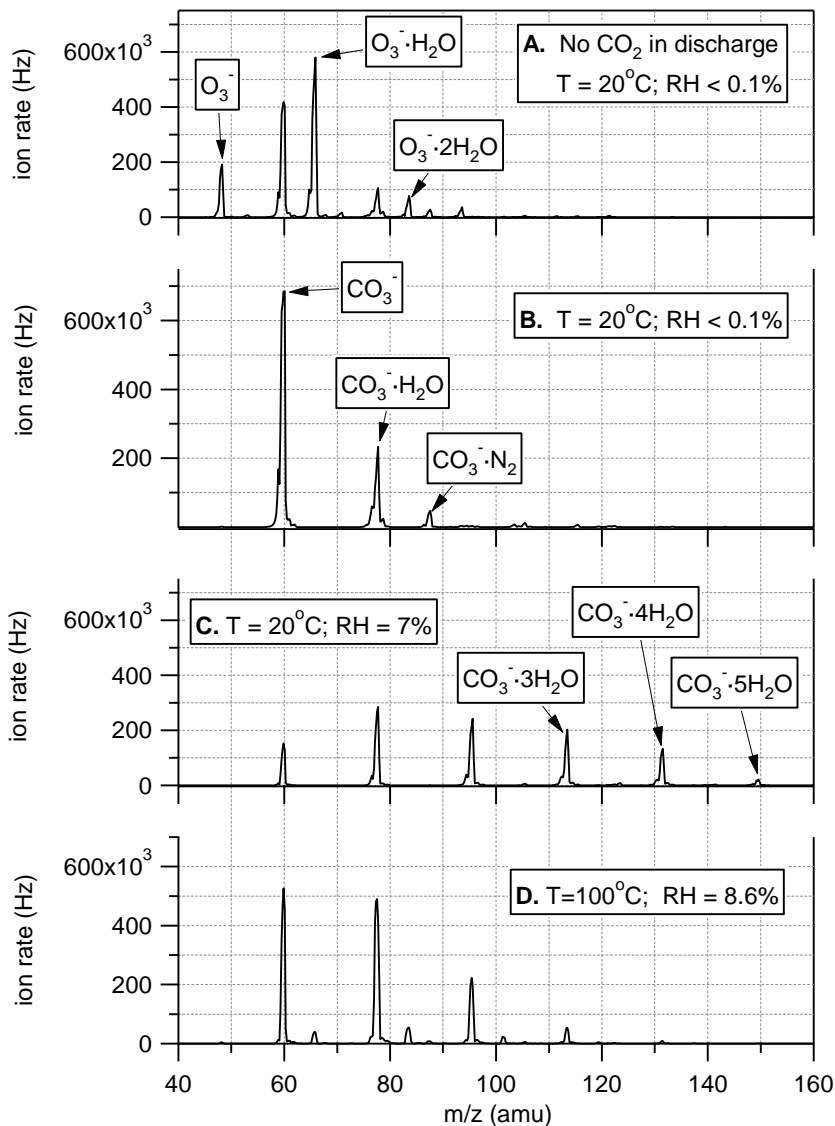


Fig. 3. Background spectra; $T_{fi} = 20^\circ\text{C}$.

tions of $\text{CO}_3^- \cdot \text{H}_2\text{O}$ and $\text{CO}_3^- \cdot 2\text{H}_2\text{O}$ are still considerable at 100°C , the improvement is significant. On one hand, it is desirable that the concentration of $\text{CO}_3^- \cdot n\text{H}_2\text{O}$ ($n = 1, 2$) be larger than that of CO_3^- , because the reaction of SO_2 with the hydrated ion is faster [32], and thus the sensitivity is increased. On the other hand, the background signals for m/z above 100 amu are considerably reduced at high temperature. This is important in order to obtain a good DL for SO_2 because the ion $\text{CO}_4^- \cdot 2\text{H}_2\text{O}$ has the same mass as SO_5^- ($m/z = 112$ amu) and hence produces an undesirable background signal. In fact, the background signal at 112 amu is three times larger at 20°C than at 100°C . The effect is more dramatic for the background signal at 130 amu (due to $\text{CO}_4^- \cdot 3\text{H}_2\text{O}$, which interferes with $\text{SO}_5^- \cdot \text{H}_2\text{O}$): the background signal at 20°C is one order of magnitude larger than the signal at 100°C . The AFRL group has demonstrated that optimization of gas flows, needle position, and corona volt-

age can minimize the signal of $\text{CO}_4^- \cdot n\text{H}_2\text{O}$ during a field experiment.

4.2. Effect of RH on SO₂ detection

Fig. 6 illustrates the detection of SO_2 under three different conditions at room temperature (no CO_2 in the ion source, at $\text{RH} < 0.1\%$, and at 4.5% RH). The background spectra and the spectra obtained when 2.7 ppb SO_2 was added to the main flow of nitrogen are compared. Under dry conditions, the main peak observed due to SO_2 is at 112 amu, which corresponds to SO_5^- . A small signal due to $\text{SO}_5^- \cdot \text{N}_2$ is also present. When water is added, SO_5^- forms clusters with water molecules, and peaks due to $\text{SO}_5^- \cdot \text{H}_2\text{O}$ and $\text{SO}_5^- \cdot 2\text{H}_2\text{O}$ are also present ($m/z = 130$ and 148 amu). The background signal at 112 amu is from $\text{CO}_4^- \cdot 2\text{H}_2\text{O}$ ions, which are also formed in the discharge.

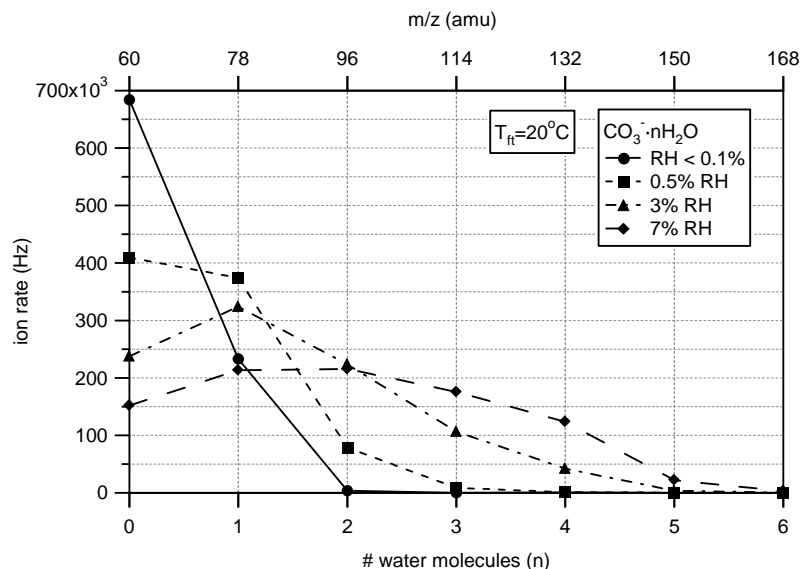


Fig. 4. $\text{CO}_3^- \cdot n\text{H}_2\text{O}$ cluster distribution at different RH in sample air (<0.1, 0.5, 3, and 7%); $T_{\text{ft}} = 20^\circ\text{C}$.

In order to confirm that the increase in the 112 amu is a result of reactions between SO_2 and the precursor ions, the signal obtained when SO_2 was added to the flow-tube (total signal minus the background signal) is plotted versus the concentration of SO_2 . Fig. 7 shows a linear correlation between these two values and confirms the suitability of the ionization scheme used.

$\text{SO}_5^- \cdot n\text{H}_2\text{O}$ ($n = 0-2$) signals normalized to SO_2 concentration (SO_2 sensitivities) are shown in Fig. 8 as a function of RH. The total SO_5^- ($\sum \text{SO}_5^- \cdot n\text{H}_2\text{O}$, $n = 0-3$) normalized signal is also shown. When water is added to the flow-tube, it forms clusters with the ions present (precursor and product) which has two effects. First, the signal of

each ion partitions into several smaller signals; in addition, the ion/molecule reaction rates of the clusters are different from those of the bare ions (see Table 1). At $\text{RH} < 5\%$, the SO_5^- signal decreases with increasing RH because the ion forms clusters with water molecules, and the ion signals of $\text{SO}_5^- \cdot \text{H}_2\text{O}$ and $\text{SO}_5^- \cdot 2\text{H}_2\text{O}$ increase. However, the total SO_5^- signal increases because there are more $\text{CO}_3^- \cdot \text{H}_2\text{O}$ ions, which react faster with SO_2 than CO_3^- does. As more water is added, higher hydrates of CO_3^- are formed. Once the reactant hydrates contain three or more water molecules, the reaction rate with SO_2 decreases sharply, and the total SO_5^- signal decreases as well. Jost et al. [34] found a qualitatively similar behavior of the sensitivity to SO_2 using an

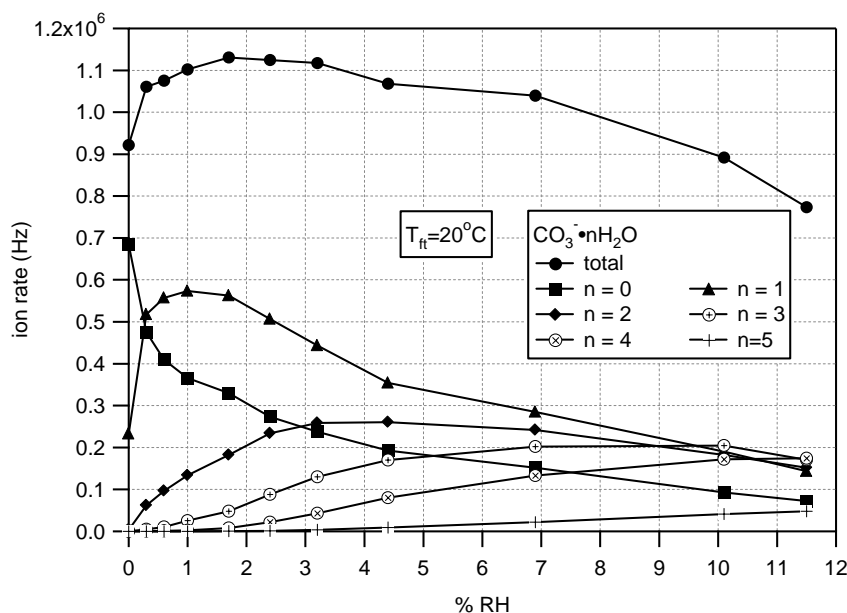


Fig. 5. Ion signal of $\text{CO}_3^- \cdot n\text{H}_2\text{O}$ as a function of RH in sample air; $T_{\text{ft}} = 20^\circ\text{C}$. The total CO_3^- ion signal ($\sum \text{CO}_3^- \cdot n\text{H}_2\text{O}$, $n = 0-6$) is also shown.

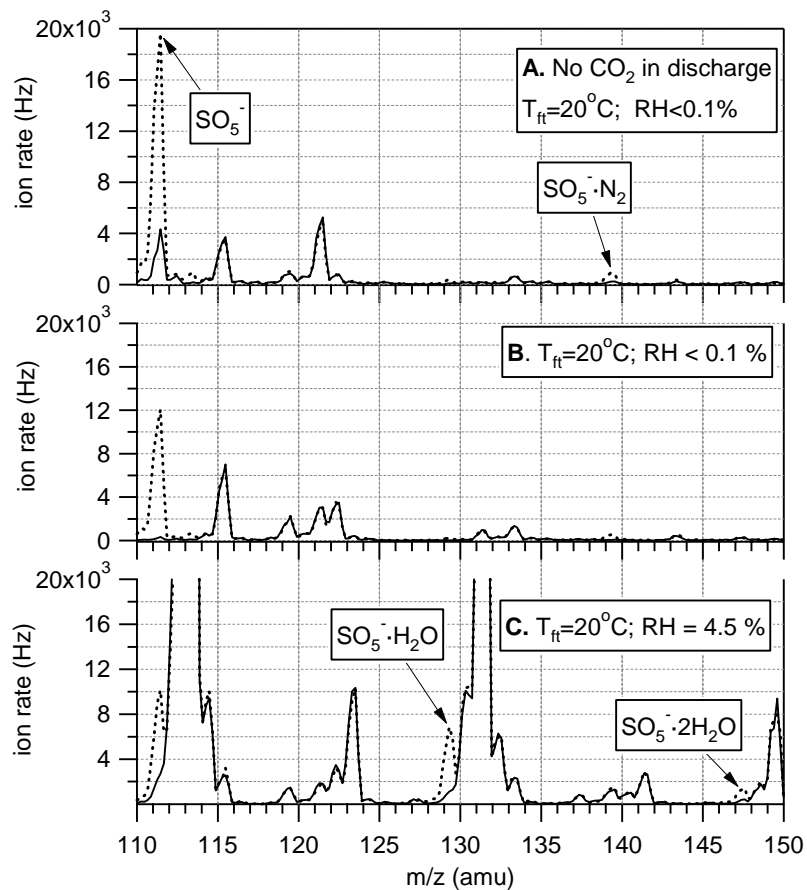


Fig. 6. Comparison of background spectra (solid line) and spectra obtained when 2.7 ppbv of SO_2 is added in the flow-tube (dotted line); $T_{\text{ft}} = 20^\circ\text{C}$. Peaks related to SO_2 detection are indicated.

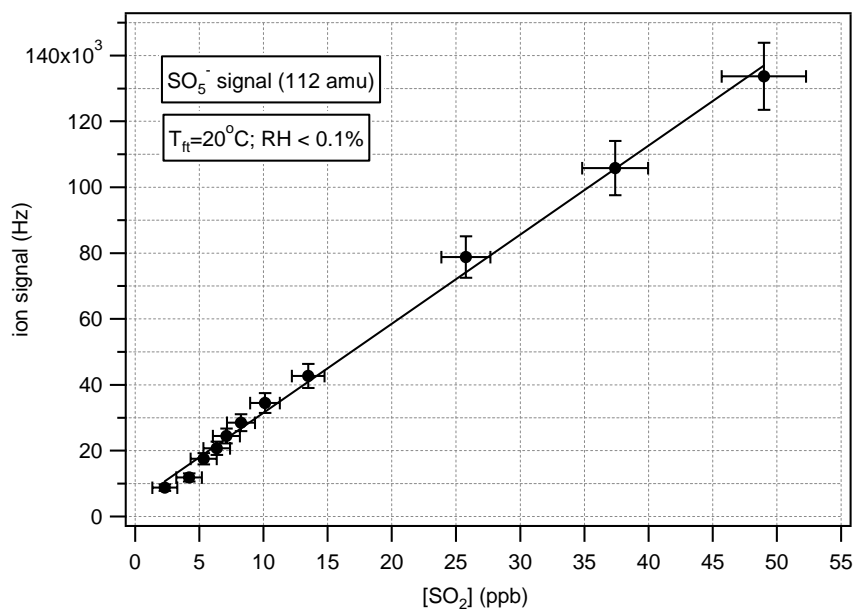


Fig. 7. SO_5^- signal as a function of SO_2 concentration at $\text{RH} < 0.1\%$ and $T_{\text{ft}} = 20^\circ\text{C}$. The line is a linear fit to the data ($r = 0.9983$).

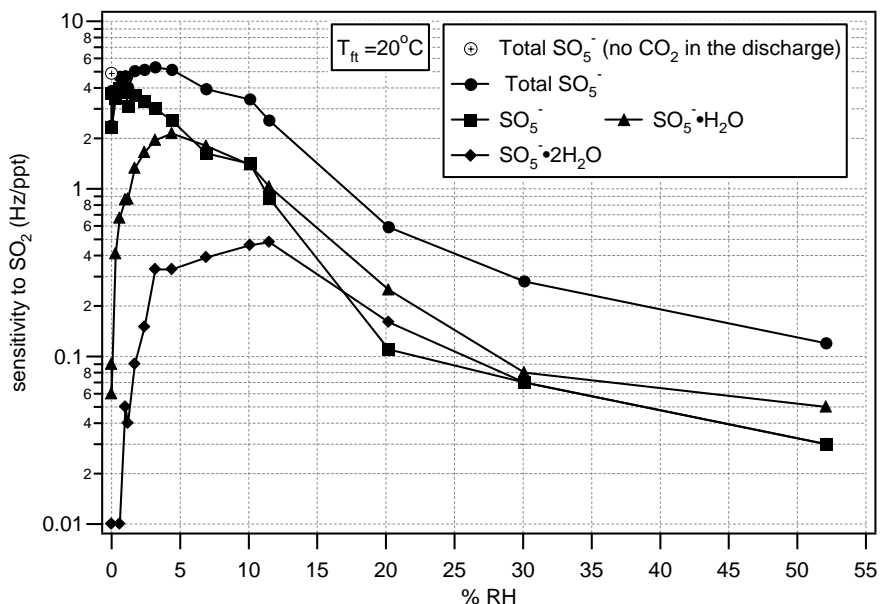


Fig. 8. Sensitivity to SO₂ as a function of RH in sample air; T_{ft} = 20°C.

atmospheric pressure chemical ionization mass spectrometer (AP-CIMS). Fig. 6 in their paper shows that there is a maximum and the sensitivity decreases slightly when very dry air is probed.

The result of heating the flow-tube is shown in Fig. 9, which is similar to Fig. 8 except for the fact that the temperature of the drying cap is 100°C. At low RH, the ion signals at 100°C are smaller than those at 20°C. However, as RH increases, the ion signal of SO₅⁻ decreases more slowly at 100°C than it does at 20°C. In fact, at 55% RH, the signal due to SO₅⁻ is almost one order of magnitude larger at 100°C than at 20°C.

Changes in sensitivity with humidity and temperature can be explained based on the following general reaction:



where the reagent ion, X_i⁻, can be O₃⁻·mH₂O (m = 0–2) or CO₃⁻·nH₂O (n = 0–5). Assuming that the fractions of SO₂ and X_i⁻ that react is small, the concentration of SO₅⁻ varies linearly with SO₂ and precursor ion concentrations:

$$[\text{SO}_5^-]_{\text{tot}} = [\text{SO}_2]t \sum k_i[\text{X}_i^-] \quad (10)$$

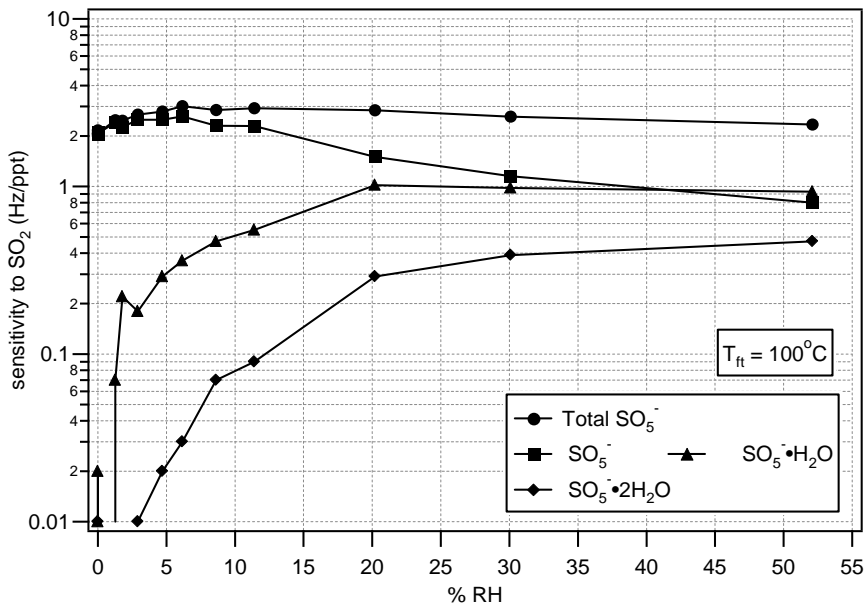


Fig. 9. Sensitivity to SO₂ as a function of RH in sample air; T_{ft} = 100°C.

where t is the reaction time, k_i is the reaction rate constant between SO_2 and X_i^- , and $[\text{SO}_5^-]_{\text{tot}}$ is the sum of all the hydrates of SO_5^- . This expression also assumes that any reverse reaction back to the reactant ions is negligible. According to Eq. (10), the signal of the product ion, $S(\text{SO}_5^-)$ must be proportional to the sum of the signal of each precursor ion, $S(\text{X}_i^-)$, times the rate constant for the reaction of SO_2 with that ion, k_i :

$$S(\text{SO}_5^-)_{\text{tot}} \propto [\text{SO}_2] \sum k_i S(\text{X}_i^-) \quad (11)$$

Values for $\sum k_i S(\text{X}_i^-)$ at 20, 40, 70, 100, and 150 °C at RH from <0.1 to 50% were calculated using measured signals, $S(\text{X}_i^-)$, for $\text{X}_i^- = \text{O}_3^- \cdot m\text{H}_2\text{O}$ ($m = 0-3$) and $\text{CO}_3^- \cdot n\text{H}_2\text{O}$ ($n = 0-5$). Rate constants measured by Möhler et al. [31] were used for $\text{O}_3^- \cdot m\text{H}_2\text{O}$. For $\text{CO}_3^- \cdot n\text{H}_2\text{O}$, rate constants from Seeley et al. [32] were used. Except for the CO_3^- reaction, which was measured up to a temperature of ~ 600 K, the rate constants used were all measured at $T_{\text{ft}} = 300$ K or below. Fig. 10A shows the sensitivity to SO_2 ($S(\text{SO}_5^-)_{\text{tot}}/[\text{SO}_2]$), where the concentration of SO_2 is expressed in molecules cm^{-3} as a function of $\sum k_i S(\text{X}_i^-)$ at 20, 40, and 70 °C. The large uncertainties on $\sum k_i S(\text{X}_i^-)$ mainly reflect the uncertainties in the reported reaction rates (25–30%), but do not include the error due to using reaction rate constants that were measured at a different temperature and assuming no temperature dependence. The error bars on the sensitivity reflect only the uncertainty in the ion signals and the flow rates measurements. Daily variations in the sensitivity resulting from changes in experimental conditions (slight changes in pressure, alignment, etc.) are not

accounted for. A linear regression fit was performed on the data in Fig. 10A, excluding the points at dry conditions (RH < 1%), which clearly deviate from a linear fit, and a slope of 0.9 ms was found. According to Eq. (10), this slope corresponds to the reaction time in the flow-tube.

In general, the data taken under dry conditions (ion signals and ratios of ion signals) do not fall on the line defined by the rest of the data in Fig. 10A. One explanation for this behavior is that the region close to the orifice at the entrance of the mass spectrometer is hotter than the flow-tube and, hence the water clusters dissociate in the vicinity of the mass spectrometer. In this case, the mass spectra would show less CO_3^- hydrates than there really were in the gas in the flow-tube (when the ion/molecule reactions took place), leading to the shift of the dry points to the left. The fact that the higher RH data follow a line is a consequence of the fact that $\text{CO}_3^- \cdot n\text{H}_2\text{O}$, $n = 1-3$ are the predominant precursor ions and they all have similar reaction rates.

Fig. 10B shows the same linear regression as in Fig. 10A together with observed ($(\text{SO}_5^-)_{\text{tot}}/[\text{SO}_2]$) versus calculated $\sum k_i S(\text{X}_i^-)$ at 100 and 150 °C. When the data points at 150 °C were measured, the drying cap had been removed. The poor fit of observations to the line in Fig. 10A likely also reflects a difference between the measured distribution of reactant ions and those present in most of the reaction region. At high temperature, the effect of this artifact is similar to the effect on dry conditions. Furthermore, at high temperature not only will the hydrate distribution change, but also the rate of conversion of O_3^- to CO_3^- will slow down [35].

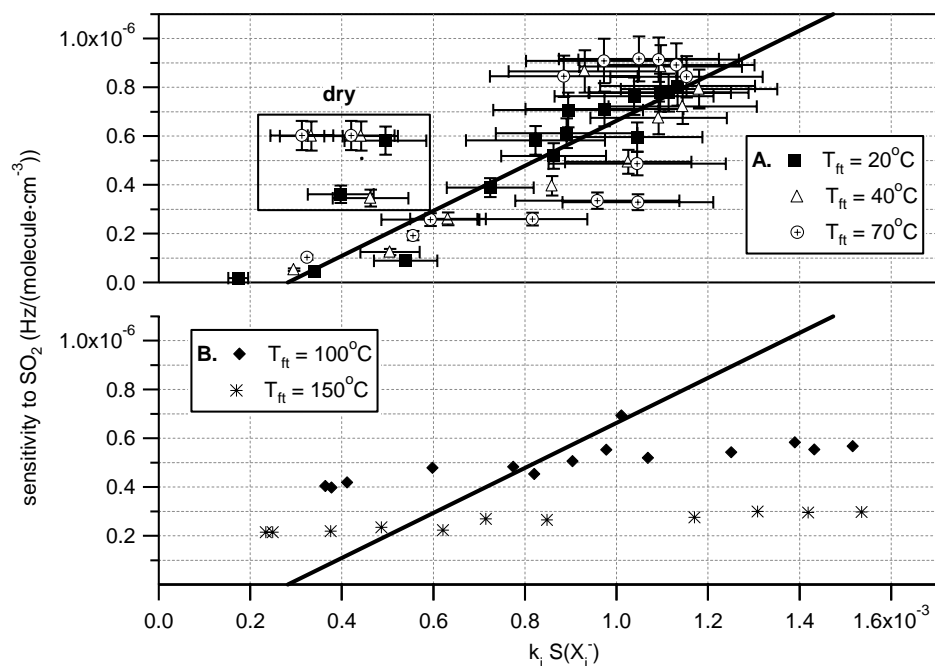


Fig. 10. Total SO_2 sensitivity as a function of the sum of the rates of reaction times the precursor ion signal. Data were taken at RH between <0.1 and 50%. (A) Data points with $T_{\text{ft}} = 20, 40,$ and 70°C . The line is a linear fit to the points outside the box ($b = -2.6 \times 10^{-7}$, $m = 9.2 \times 10^{-4}$, $r = 0.8590$). (B) Data points with $T_{\text{ft}} = 100$ and 150°C . The line is the same line as in (A).

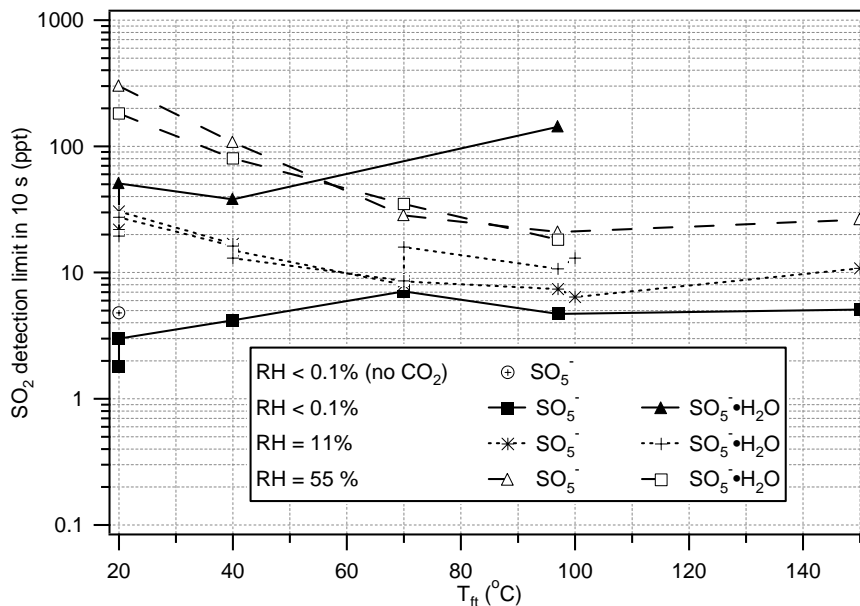


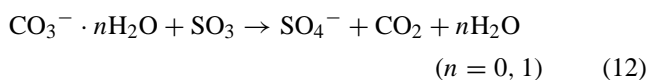
Fig. 11. Detection limit of SO_2 over 10 s integration time using SO_5^- (112 amu) and $SO_5^- \cdot H_2O$ (130 amu) as a function of temperature of the drying cap (T_{fit}) for three different RH in sample air (<math>< 0.1, 11, \text{ and } 55\%</math>).

Overall, these results show that, at high relative humidity, an increase in the temperature can improve the sensitivity to SO_2 . Increasing temperature also has a positive effect on the DL of SO_2 . Fig. 11 shows the effect of the flow-tube temperature on the DL of the instrument (with 10 s integration time) for three different RH values. At 20 °C, the DL of SO_2 is lower when CO_2 is added to the discharge, even though the signal of SO_5^- is larger in the absence of CO_2 (see Fig. 8). The reason is that the background signal at 112 amu is smaller when CO_2 is added into the discharge. At the lowest RH, the DL deteriorates with temperature; however, at high RH, the DL actually improves up to one order of magnitude as the temperature increases. Also, the DL using SO_5^- or $SO_5^- \cdot H_2O$ as the product ion to be detected is very similar.

4.3. Effect of RH on H_2SO_4 detection

All the data described in this section were obtained without the drying cap in the flow-tube and at a temperature measured at the copper flange of 150 °C. The temperature of the gas in the flow-tube (measured in front of the discharge) was 110 ± 2 °C.

Fig. 12 compares background spectra with spectra obtained when a calculated value of 16 ppbv sulfuric acid is introduced into the flow-tube at different values of RH. Under dry conditions two signals are prominent in the spectra, one at $m/z = 96$ and the other at 97 amu. The signal at 97 amu corresponds to HSO_4^- from reaction (7). The signal at $m/z = 96$ amu is due to SO_4^- , according to the following reaction reported by Arnold et al. [36]:



SO_3 is produced from the dissociation of H_2SO_4 , which is favored at high temperatures and low water concentration. As the relative humidity in the flow-tube increases, the relative signal level from SO_4^- (96 amu) compared to HSO_4^- (97 amu) decreases, as the equilibrium $H_2SO_4 \leftrightarrow SO_3 + H_2O$ shifts back towards the reactant. However, the back-

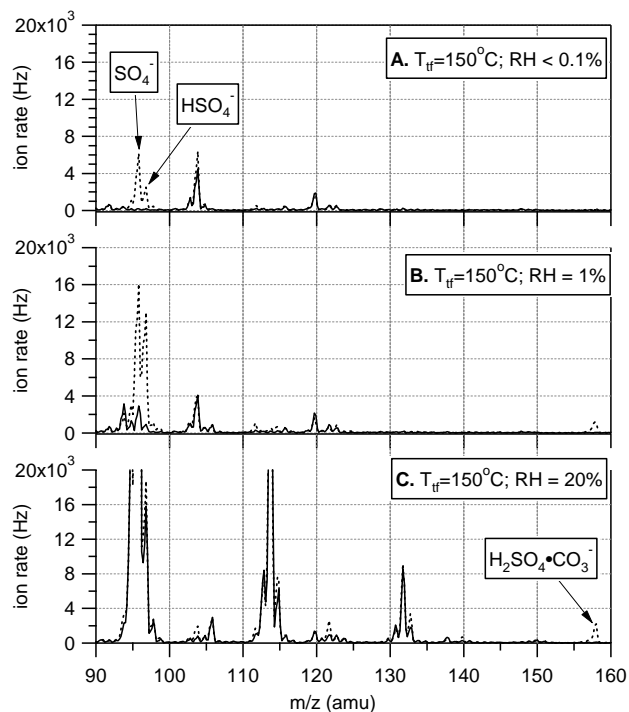


Fig. 12. Comparison of background spectra (solid line) and spectra obtained when 16 ppbv of H_2SO_4 is added in the flow-tube (dashed line). These spectra were taken at $T_{fit} = 150$ °C and without the drying cap.

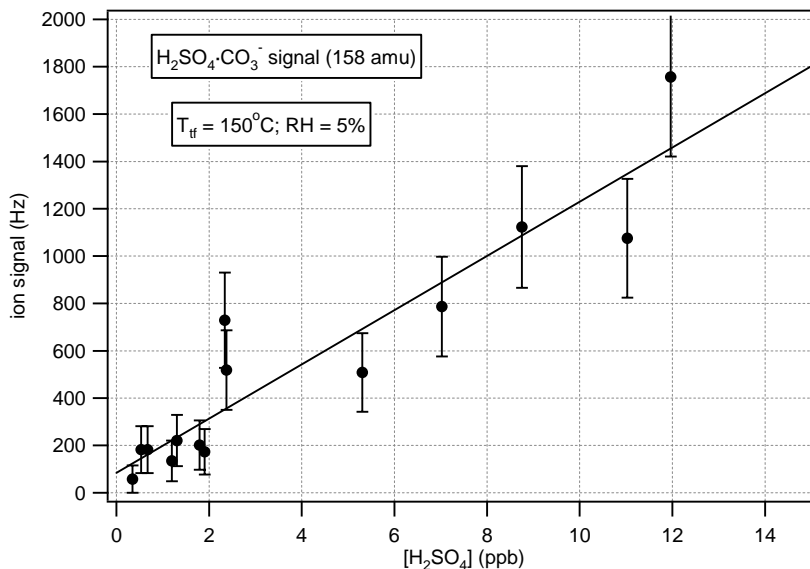


Fig. 13. $\text{H}_2\text{SO}_4\text{-CO}_3^-$ signal as a function of sulfuric acid concentration in the flow-tube at $\text{RH} = 5\%$ and $T_{\text{ft}} = 150^\circ\text{C}$. The line is a linear fit to the data ($r = 0.9326$).

ground signals at $m/z = 96$ and 97 amu (due to $\text{CO}_3^- \cdot 2\text{H}_2\text{O}$ and its isotope) increase and the signals from SO_4^- and HSO_4^- are not detectable at $\text{RH} > 5\%$. Hence, at high relative humidity, it is not practical to use either of these product ions to detect sulfuric acid.

In Fig. 12, for $\text{RH} = 1\%$ and above, a signal at $m/z = 158$ amu is also visible, which is due to $\text{H}_2\text{SO}_4\text{-CO}_3^-$ (see reaction (8)). The increase in this signal at high water vapor concentrations in the flow-tube is convenient for detecting sulfuric acid at high relative humidity. Furthermore, the small background signal at 158 amu, even at high RH, gives a low DL at high concentration water vapor. To confirm that the peak at 158 amu is indeed due to sulfuric acid, the signal at $\text{RH} = 5\%$ (after the background signal was subtracted) is shown in Fig. 13 against the concentration of sulfuric acid calculated from the impinger model. The data

in Fig. 13 were taken at various temperatures (between 20 and 46°C) of the H_2SO_4 solution in the impinger and with different flows (from 100 to 350 sccm) over the solution. Although we cannot assess the value of the uncertainty in the concentration of sulfuric acid introduced in the flow-tube, the linear correlation obtained indicates that, at least, the sulfuric acid source is reproducible. Fig. 13 also confirms that the ionization scheme proposed is adequate for H_2SO_4 detection.

Sensitivities to H_2SO_4 using the signal at $m/z = 158$ amu were calculated as a function of RH and are shown in Fig. 15. Sensitivity to SO_2 under the same conditions is also shown for comparison. Because of the uncertainty of the sulfuric acid source, the sensitivity to the acid in Fig. 14 is only a lower limit. Contrary to SO_2 , the sensitivity to H_2SO_4 improves as the water concentration increases.

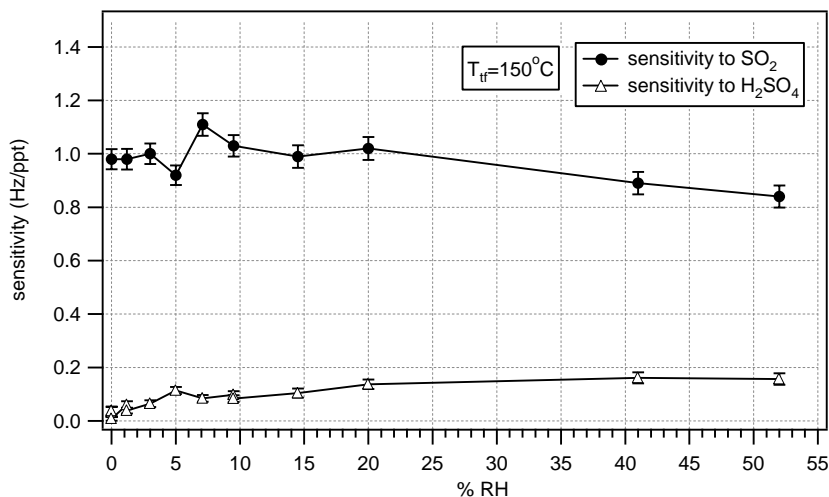


Fig. 14. Sensitivities of SO_2 and H_2SO_4 as a function of RH of sample air at $T_{\text{ft}} = 150^\circ\text{C}$.

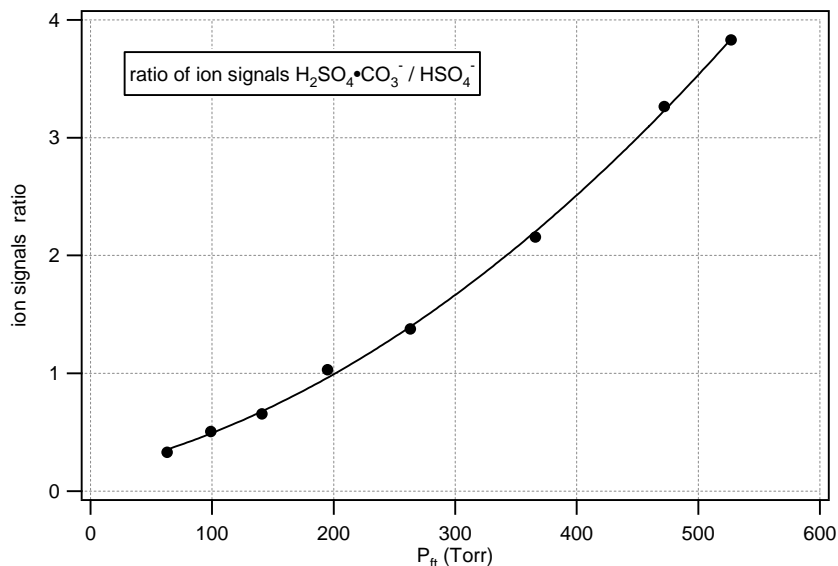


Fig. 15. Ratio of ion signal of $\text{H}_2\text{SO}_4\text{-CO}_3^-$ (158 amu) and ion signal of HSO_4^- (97 amu) as a function of pressure in the flow-tube; $T_{\text{ft}} \approx 27^\circ\text{C}$. The line is for visual reference only.

The pressure dependence of reactions (7) and (8) was studied by the AFRL group using a similar instrument to the one described above with the same ionization scheme. During the experiment, sulfuric acid was introduced in the flow-tube using dry nitrogen as the carrier gas, while the pressure was changed. The temperature of the flow-tube was kept constant at approximately 28°C . The ratio of the ion signal of $\text{H}_2\text{SO}_4\text{-CO}_3^-$ (158 amu) over the ion signal of HSO_4^- (97 amu) as a function of pressure is plotted in Fig. 15. This Figure shows that the relative ion signal for $\text{H}_2\text{SO}_4\text{-CO}_3^-$ increases as the pressure increases.

The effects of RH and pressure on reactions (7) and (8) described above indicate that reaction (8) is a promising ionization scheme for the detection of sulfuric acid using CIMS. However, more work is needed in order to determine the conditions that optimize the sensitivity to H_2SO_4 .

5. Conclusions

High relative humidity has a negative effect on the sensitivity of the CIMS to SO_2 and H_2SO_4 because water molecules form clusters with the reactant and product ions. The effect can be avoided by increasing the temperature.

For the detection of SO_2 at high relative humidity, SO_5^- or $\text{SO}_5^- \cdot \text{H}_2\text{O}$ can be used as product ions, with roughly the same sensitivity and DL.

It is proposed to use a new ionization scheme for sulfuric acid using the product ion $\text{H}_2\text{SO}_4\text{-CO}_3^-$ ($m/z = 158$ amu) to detect the acid. The background signal at 158 amu is small, and a better DL can be achieved than if the product ion is HSO_4^- .

Acknowledgements

We appreciate the assistance from personnel of the Air Force Research Laboratory: J. Borghetti, and F. Federico. We thank Jonathan O. Allen for providing us with the impinger model. This work was supported by Office of Naval Research contract N00014-97-C-0254 and grant N00014-96-1-0119, and by Aerodyne Research IR&D funds. We thank R.T. Bluth of the Naval Postgraduate School, R.J. Ferek of the Office on Naval Research, and C.E. Kolb of Aerodyne Research for their support.

References

- [1] H. Berresheim, P.H. Wine, D.D. Davis, in: H.B. Singh (Ed.), *Composition, Chemistry, and Climate of the Atmosphere*, Van Nostrand Reinhold, New York, 1995, p. 251.
- [2] M. Kulmala, L. Pirjola, J.M. Mäkelä, *Nature* 404 (2000) 66.
- [3] R.J. Charlson, S.E. Schwartz, J.M. Hales, R.D. Cess, J.A. Coakley, J.E. Hansen, D.J. Hofmann, *Science* 255 (1992) 423.
- [4] J.H. Seinfeld, S.N. Pandis, *Atmospheric Chemistry and Physics. From Air Pollution to Climate Change*, Wiley, USA, 1998.
- [5] W.R. Stockwell, J.G. Calvert, *Atmos. Environ.* 17 (1983) 2231.
- [6] J.T. Jayne, U. Pöschl, Y. Chen, D. Dai, L.T. Molina, D.R. Worsnop, C.E. Kolb, M.J. Molina, *J. Phys. Chem. A* 101 (1997) 10000.
- [7] K.S. Carslaw, S.L. Clegg, P. Brimblecombe, *J. Phys. Chem. A* 99 (1995) 11557.
- [8] H. Berresheim, F.L. Eisele, D.J. Tanner, L.M. McInnes, D.C. Ramsey-Bell, D.S. Covert, *J. Geophys. Res.* 98 (1993) 12701.
- [9] H. Berresheim, T. Elste, C. Plass-Dülmer, F.L. Eisele, D.J. Tanner, *Int. J. Mass Spectrom.* 202 (2000) 91.
- [10] P.H. Daum, S.R. Springston, in: L. Newman (Ed.), *Measurement Challenges in Atmospheric Chemistry*, vol. 232, American Chemical Society, Washington, DC, 1993, p. 101.

- [11] B.J. Finlayson-Pitts, J. James N. Pitts, *Chemistry of the Upper and Lower Atmosphere: Theory, Experiments, and Applications*, Academic Press, New York, 2000.
- [12] D.E. Hunton, J.O. Ballenthin, J.F. Borghetti, G.S. Federico, T.M. Miller, W.F. Thorn, A.A. Viggiano, B.E. Anderson, W.R. Cofer, D.S. McDougal, C.C. Wey, *J. Geophys. Res.* 105 (2000) 26841.
- [13] A. Laaksonen, L. Pirjola, M. Kulmala, K.H. Wohlfrom, F. Arnold, F. Raes, *J. Geophys. Res.* 105 (2000) 1459.
- [14] O. Möhler, F. Arnold, *Geophys. Res. Lett.* 19 (1992) 1763.
- [15] T. Reiner, D. Sprung, C. Jost, R. Gabriel, O.L. Mayol-Bracero, M.O. Andreae, T.L. Campos, R.E. Shetter, *J. Geophys. Res.* 106 (2001) 28.
- [16] D. Sprung, C. Jost, T. Reiner, A. Hansel, A. Wisthaler, *J. Geophys. Res.* 106 (2001) 28.
- [17] F. Arnold, R. Fabian, *Nature* 283 (1980) 105.
- [18] F.L. Eisele, D.J. Tanner, *J. Geophys. Res.* 98 (1993) 9001.
- [19] V.L. Talrose, P.S. Vinogradov, I.K. Larin, in: M.T. Bowers (Ed.), *Gas Phase Ion Chemistry*, vol. 1, Academic Press, New York, 1979, p. 305.
- [20] S.T. Arnold, R.A. Morris, A.A. Viggiano, *J. Chem. Phys.* 103 (1995) 2454.
- [21] A.A. Viggiano, J.V. Seeley, P.L. Mundis, J.S. Williamson, R.A. Morris, *J. Phys. Chem. A* 101 (1997) 8275.
- [22] Y. Ikezoe, S. Matsuoka, M. Takebe, A.A. Viggiano, *Gas Phase Ion-Molecule Reaction Rate Constants Through 1986*, Maruzen, Tokio, 1987.
- [23] A.A. Viggiano, S.T. Arnold, R.A. Morris, *Int. Rev. Phys. Chem.* 17 (1998) 147.
- [24] A.A. Viggiano, D.E. Hunton, *J. Mass Spectrom.* 34 (1999) 1107.
- [25] R.C. Miake-Lye, B.E. Anderson, W.R. Cofer, H.A. Wallio, G.D. Nowicki, J.O. Ballenthin, D.E. Hunton, W.B. Knighton, T.M. Miller, J.V. Seeley, A.A. Viggiano, *Geophys. Res. Lett.* 25 (1998) 1677.
- [26] T.M. Miller, J.O. Ballenthin, R.F. Meads, D.E. Hunton, W.F. Thorn, A.A. Viggiano, Y. Kondo, M. Koike, Y. Zhao, *J. Geophys. Res.* 105 (2000) 3701.
- [27] P.H. Dawson, in: P.H. Dawson (Ed.), *Quadrupole Mass Spectrometry and its Applications*, American Institute of Physics, Woodbury, NY, 1995, p. 95.
- [28] J.O. Allen, A.F. Sarofim, K.A. Smith, *Aerosol Sci. Tech.* (2000), in preparation.
- [29] E.E. Ferguson, F.C. Ferguson, D.L. Albritton, in: M.T. Bowers (Ed.), *Gas Phase Ion Chemistry*, vol. 1, Academic Press, New York, 1979, p. 45.
- [30] D.L. Albritton, I. Dotan, G.E. Streit, D.W. Fahey, F.C. Fehsenfeld, E.E. Ferguson, *J. Chem. Phys.* 78 (1983) 6614.
- [31] O. Möhler, T. Reiner, F. Arnold, *J. Chem. Phys.* 97 (1992) 8233.
- [32] J.V. Seeley, R.A. Morris, A.A. Viggiano, *Geophys. Res. Lett.* 24 (1997) 1379.
- [33] P.W. Villalta, R.C. Miake-Lye, C.E. Kolb, A chemical ionization mass spectrometer instrument for measurement of aerosol precursors in the National Oceanic Partnership Program's field study at Calspan, Buffalo, NSF Final Report Grant ATM 9814068, 2000.
- [34] C. Jost, D. Sprung, T. Kenntner, T. Reiner, *Int. J. Mass Spectrom.* 223/224 (2003) 771.
- [35] I. Dotan, J.A. Davidson, G.E. Streit, D.L. Albritton, F.C. Fehsenfeld, *J. Chem. Phys.* 67 (1977) 2874.
- [36] S.T. Arnold, R.A. Morris, A.A. Viggiano, J.T. Jayne, *J. Geophys. Res.* 100 (1995) 14141.